# FYN-TRAF3IP2 and KHDRBS1-LCK hijack T cell receptor signaling in peripheral T cell lymphoma, not otherwise specified

**Koen Debackere**
KU Leuven
**Lukas Marcelis**
KU Leuven
**Sofie Demeyer**
KU Leuven
**Marlies Vanden Bempt**
KU Leuven https://orcid.org/0000-0003-0111-0263
**Nicole Mentens**
KU Leuven
**Olga Gielen**
KU Leuven
**Kris Jacobs**
KU Leuven
**Michael Broux**
Flanders Institute for Biotechnology
**Gregor Verhoef**
Universitaire Ziekenhuizen Leuven
**Lucienne Michaux**
KU Leuven
**Carlos Graux**
CHU Dinant Godinne UCL Namur
**Iwona Wlodarska**
KU Leuven
**Philippe Gaulard**
INSERM
**Laurence de Leval**
Lausanne University Hospital https://orcid.org/0000-0003-3994-516X
**Thomas Tousseyn**
Universitaire Ziekenhuizen Leuven
**Jan Cools** ( jan.cools@kuleuven.be )

KU Leuven/VIB

**Daan Dierickx**

Universitaire Ziekenhuizen Leuven

---

**Article**

**Keywords:** Peripheral T cell lymphoma (PTCL), non-Hodgkin lymphomas, T cell receptor (TCR)

**Posted Date:** February 5th, 2021

**DOI:** https://doi.org/10.21203/rs.3.rs-200114/v1



---

**Version of Record:** A version of this preprint was published at Nature Communications on June 17th, 2021. See the published version at https://doi.org/10.1038/s41467-021-24037-4.

# Abstract

Peripheral T cell lymphoma (PTCL) is a heterogeneous group of non-Hodgkin lymphomas with poor prognosis. Up to 30% of PTCL lack distinctive features and are classified as PTCL, not otherwise specified (PTCL-NOS). To further improve our understanding of the genetic landscape and biology of PTCL-NOS, we performed RNA-sequencing of 18 cases and validated results in an independent cohort of 37 PTCL cases. We identified FYN-TRAF3IP2, KHDRBS1-LCK and SIN3A-FOXO1 as new in-frame fusion transcripts, with FYN-TRAF3IP2 as a recurrent fusion detected in 8 of 55 cases. Using ex vivo and in vivo experiments, we demonstrate that FYN-TRAF3IP2 and KHDRBS1-LCK activate signaling pathways downstream of the T cell receptor (TCR) complex and confer therapeutic vulnerability to clinically available drugs.


# Introduction

Peripheral T cell lymphoma (PTCL) arises from post-thymic mature T lymphocytes. PTCL comprises 10 to 20% of non-Hodgkin lymphomas, depending on geographical variation. With the exception of *ALK*- and *DUSP22*-translocated anaplastic large cell lymphoma (ALCL)[1], the outcome with current therapies is unsatisfactory[2]. Up to 30% of PTCL cases lack distinctive features and are classified as PTCL not otherwise specified (PTCL-NOS). Five-year overall survival for PTCL-NOS has stagnated at 30% and guidelines for first-line treatment recommend to treat patients with PTCL-NOS in the context of a clinical trial[2,3]. Although efforts have been made to study the genetic landscape of PTCL-NOS[4–6], the disease biology remains poorly characterized, which hampers the rational design of new clinical trials.

Engagement of immunoreceptors elicits a brisk proliferative and metabolic response in B cells and T cells. This response is intensely intertwined with the Nuclear Factor Kappa light chain enhancer of activated B cells (NF-κB) pathway. Oncogenic activation of the NF-κB pathway by somatic single nucleotide variants and copy number variants is frequent in activated B-cell-like diffuse large B cell lymphoma[7]. With the notable exception of translocations involving *MALT1* in mucosa-associated lymphoid tissue lymphoma and an *ITK-SYK* gene fusion in peripheral T cell lymphoma with a T follicular helper phenotype (PTCL-TFH)[8], activation of the NF-κB pathway by gene fusions is rare[7]. On the whole, gene fusions are recurrent disease drivers in hematological malignancies of both lymphoid and myeloid origin. A subset of gene fusions gives rise to chimeric proteins with altered kinase activity or specificity, altered transcriptional regulation or altered post-translational regulation[9,10]. Chimeric transcripts are distinctive disease features with a pivotal role in oncogenesis and have also been identified in PTCL[8,11–14]. These features render them ideal candidates for therapeutic intervention.

In this study, we identify two novel chimeric transcripts in a cohort of PTCL-NOS that hijack signaling pathways downstream of the T cell receptor (TCR) complex. We describe a recurrent *FYN-TRAF3IP2* fusion transcript in PTCL-NOS and PTCL-TFH and a *KHDRBS1-LCK* fusion transcript in PTCL-NOS. Furthermore, we show that both transcripts confer therapeutic vulnerability to clinically available drugs.

# Results

### Transcriptome sequencing identifies novel fusion transcripts in PTCL-NOS

To identify fusion events in PTCL-NOS, we performed high coverage, paired-end RNA sequencing (RNA-seq) on a cohort of 15 PTCL-NOS (**Supplementary Table 1**) cases and 3 PTCL-TFH[13]. Gene expression analysis indicated expression of T follicular helper ($T_{fh}$) markers in the PTCL-TFH cases (**Supplementary Fig. 1a**). In agreement with the histopathological diagnosis, a subset of PTCL-NOS cases expressed *TNFRSF8* (CD30). Expression of the ALCL marker genes *BATF3* and *TMOD1*[15] clearly separated the PTCL-NOS cases from ALCL cases[12] (**Supplementary Fig. 1b**).

In 5 cases, we detected fusion transcripts, including the *VAV1-MYO1F* and *TBL1XR1-TP63* fusions that were reported previously in PTCL-NOS[11,16], and further confirm the validity of this cohort. In addition, we identified 3 novel in-frame fusion transcripts: *FYN-TRAF3IP2* (2 cases), *KHDRBS1-LCK* (1 case) and *SIN3A-FOXO1* (1 case) (**Supplementary Fig. 1c**). We found evidence for a gene fusion between the neighboring *FYN* and *TRAF3IP2* genes in 1/15 PTCL-NOS (case PTCL2) and 1/3 PTCL-TFH (case FTCL4). In the PTCL-NOS case, exon 7 of *FYN* was fused to exon 3 of *TRAF3IP2* (Fig. 1a). To exclude that such fusion was the result of transcriptional read-through, we investigated the genomic region by long range PCR and we identified an interstitial deletion of 92597 bp on chromosome 6 (Fig. 1b). In the PTCL-TFH case, exon 8 of *FYN* was fused to exon 3 of *TRAF3IP2* (Fig. 1a). In both variants of the fusion protein, the FYN moiety contained the membrane localization motif (SH4 domain) and the SH3 domain of FYN, but lacked the FYN tyrosine kinase domain. The TRAF3IP2 moiety consisted of the almost complete open reading frame, only lacking the first 7 amino acids and thus retaining the TNF receptor associated factor 6 (TRAF6) binding domain in the fusion protein. Additionally, we discovered a *KHDRBS1-LCK* gene fusion that was caused by an interstitial deletion on chromosome 1 in 1/15 PTCL-NOS (case PTCL17). This gene fusion generated a chimeric transcript in which exon 3 of *KHDRBS1* was fused to exon 3 of *LCK*, resulting in the fusion of the QUA1 and K homology (KH) dimerization domains of KHDRBS1[17] to the SH3, SH2 and kinase domains of LCK (Fig. 1c).

To validate the importance of these fusion genes, we tested the presence of the *FYN-TRAF3IP2* and the *KHDRBS1-LCK* fusion genes with RT-PCR in an independent validation cohort of 37 PTCL cases (30 PTCL-NOS, 6 PTCL-TFH, 1 Adult T-cell leukemia/lymphoma (ATLL)). This screen confirmed that the *FYN-TRAF3IP2* fusion is highly recurrent as it was detected (and verified by Sanger sequencing) in 6/37 (3 PTCL-NOS, 3 PTCL-TFH) samples (**Supplementary Fig. 1d-e, Supplementary Table 2**). We detected no additional cases of the *KHDRBS1-LCK* fusion in the independent validation cohort.

### FYN-TRAF3IP2-dependent signaling intersects with TCR signaling

To study the oncogenic properties of the FYN-TRAF3IP2 fusion protein, we cloned the open reading frame (ORF) derived from patient cDNA (case PTCL2) in a bicistronic pMSCV vector with an IRES-GFP reporter (pMIG). As controls, full length *TRAF3IP2* and the N-terminal fragment of *FYN* containing the membrane localization motif, the SH3 domain and a truncated SH2 domain ($FYN^{1-232}$) were cloned in the pMIG

vector (**Supplementary Fig. 2a**). Only retroviral transduction of interleukin-3 (IL-3) dependent Ba/F3 cells with the *FYN-TRAF3IP2* ORF conferred IL-3 independent growth *in vitro*, indicating that the FYN-TRAF3IP2 fusion protein is endowed with oncogenic properties and that the combined signaling properties of both fusion partners are required (Fig. 2a).

The oncogenic signaling properties of the FYN-TRAF3IP2 fusion protein could not be related to tyrosine kinase signaling of the FYN kinase domain since it was not retained in the fusion protein. Instead, it was only the N-terminal part of FYN that was fused to the majority of the TRAF3IP2 protein. Under physiological circumstances, TRAF3IP2 is essential for IL-17 signaling. Upon engagement of the heterodimeric IL-17RA/IL-17RC complex, TRAF3IP2 translocates to the juxtamembrane compartment via homotypic SEFIR domain interactions and relays signals to the canonical NF-κB pathway and mitogen-activated protein kinase (MAPK) pathways[18]. *IL-17RA* is ubiquitously expressed, but *IL-17RC* expression is more restricted and defines the cellular response to IL-17[18]. Neither T cells from healthy volunteers (**Supplementary Fig. 2b**), nor any of the lymphoma samples in our cohort (**Supplementary Fig. 2c**) expressed *IL17RC*. Accordingly, the levels of TRAF3IP2-regulated transcripts in naive $CD4^+$ T cells transduced with empty pMIG vector (EV), pMIG-*TRAF3IP2* or pMIG-*FYN-TRAF3IP2* were primarily determined by expression of *FYN-TRAF3IP2*. Stimulation with IL-17 had an additive rather than a synergistic effect on the expression TRAF3IP2-regulated transcripts (Fig. 2b). Combined, these data strongly suggest that the biological activity of the FYN-TRAF3IP2 fusion protein did not depend on IL-17 signaling.

Given that TCR signaling is a nexus in the integrated control of proliferation and survival in healthy and malignant T cells and TRAF3IP2 activates NF-kB signaling and Mitogen-Activated Protein Kinase (MAPK) downstream of the IL-17 receptor, we hypothesized that aberrant FYN-TRAF3IP2 signaling would intersect with NF-kB signaling and MAPK signaling downstream of the TCR. We transduced the Jurkat T ALL cell line to induce the expression of *TRAF3IP2* or *FYN-TRAF3IP2*. Western blot analysis revealed increased Ser536 phosphorylation of the NF-kB subunit p65 (also known as RelA), indicative of increased activation of the canonical NF-kB pathway. Processing of p100 to p52 and Ser866/870 phosphorylation of p100 did not provide evidence for activation of non-canonical NF-kB signaling (Fig. 2c). Next, we generated a dual GFP/luciferase NF-kB reporter Jurkat cell line to measure NF-kB transcriptional activity. Cells transduced with pMSCV-*FYN-TRAF3IP2*-IRES-*mCherry* (pMImC-*FYN-TRAF3IP2)* had increased NF-kB transcriptional activity in resting conditions and after TCR stimulation with an agonistic CD3 antibody compared to Jurkat cells transduced with pMImC-$FYN^{1-232}$ or pMImC-*TRAF3IP2* (Fig. 2d). In contrast, we found no evidence for increased activation of MAPK signaling pathways (Fig. 2e).

Finally, we transduced murine $CD4^+$ T cells to express *TRAF3IP2* or *FYN-TRAF3IP2* (**Supplementary Fig. 3a**). Intracellular flow cytometry indicated increased activation of canonical NF-kB signaling by means of increased Inhibitor of NF-kB alpha (IkBa) degradation and increased Ser536 phosphorylation of p65 (Fig. 2f). There was no evidence for enhanced activation of proximal TCR signaling (ZAP70 Tyr318 phosphorylation) or increased MAPK signaling (Fig. 2g).

In summary, these data show that FYN-TRAF3IP2 activates canonical NF-kB signaling independent of IL-17.

**FYN-TRAF3IP2 localizes to the cell membrane and activates the NF-kB pathway**

Ligation of the TCR engenders the formation of a multiprotein signalosome at the membrane-cytoplasm interface. The Src-family kinases FYN and LCK are critical for proximal TCR signaling and are anchored to the plasma membrane by acylation of the unique N-terminal SH4 domains. FYN is myristoylated at Gly2, followed by palmitoylation at Cys3[19]. IL-17 dependent recruitment of TRAF3IP2 to the plasma membrane initiates signaling downstream of TRAF3IP2. Taken together, we reasoned that acylation of FYN-TRAF3IP2 would anchor the fusion protein to the plasma membrane and mediate chronic active TRAF3IP2-dependent signaling.

To this end, we mutated the N-terminal Gly2 of FYN to Ala (FYN$^{G2A}$-TRAF3IP2) to abolish acylation of the N-terminal FYN domain. Immunofluorescence imaging of 293T cells transfected with either wild-type *TRAF3IP2*, *FYN-TRAF3IP2* or *FYN$^{G2A}$-TRAF3IP*, confirmed that wild-type TRAF3IP2 resided in the cytosol, FYN-TRAF3IP2 segregated to the plasma membrane and FYN$^{G2A}$-TRAF3IP2 resulted in the redistribution of the fusion protein to the cytosol (Fig. 3a). The subcellular compartmentalization of FYN-TRAF3IP2 and FYN$^{G2A}$-TRAF3IP2 was confirmed in Ba/F3 cells (**Supplementary Fig. 3b**) and Ba/F3 cells transduced to express *FYN$^{G2A}$-TRAF3IP2*, were no longer able to grow out in the absence of IL-3 (Fig. 3b).

Next, we collected cytosolic and membrane fractions of Jurkat cells with ectopic expression of *TRAF3IP2*, *FYN-TRAF3IP2* or *FYN$^{G2A}$-TRAF3IP2* and confirmed that disruption of FYN myristoylation impeded incorporation of the fusion protein in the plasma membrane (Fig. 3c). Delocalization from the plasma membrane impaired the ability of FYN$^{G2A}$-TRAF3IP2 to activate NF-kB transcriptional activity compared to FYN-TRAF3IP2 (Fig. 3d). Likewise, immunofluorescence analysis of CD4$^{+}$ T cells displayed association of FYN-TRAF3IP2 but not TRAF3IP2 or FYN$^{G2A}$-TRAF3IP2 with the cell membrane (Fig. 3e). Exclusion of FYN-TRAF3IP2 from the membrane compartment, impaired activation of NF-kB signaling in CD4$^{+}$ T cells (Fig. 3f).

Together, these experiments demonstrate that acylation of the N-terminal SH4 domain of FYN anchors the FYN-TRAF3IP2 fusion protein to the plasma membrane. Partitioning of FYN-TRAF3IP2 to the plasma membrane is required for downstream activation of NF-kB signaling.

**FYN-TRAF3IP2 activates TRAF6 independent of the CBM signalosome**

Activation of the NF-kB pathway downstream of the TCR is initiated by protein kinase C q (PKCq)-dependent assembly of a signalosome composed of CARD11, BCL10 and MALT1 (CBM signalosome). The CBM signalosome recruits TRAF6, which leads to lysine 63-linked (K63-linked) polyubiquitination of TRAF6. K63-linked polyubiquitinated TRAF6 acts as a scaffold for the IkB Kinase (IKK) complex and Transforming-growth-factor-b-Activated Kinase 1 (TAK1) complex which will ultimately lead to the release of NF-kB transcription factors from IkB[20]. The TRAF3IP2 protein comprises an N-terminal TRAF6 binding

motif[21] and has a U-box domain with E3 ubiquitin ligase enzymatic activity through which it catalyzes K63-linked polyubiquitination of TRAF6[22] (Fig. 1a). We assumed that the interaction of the FYN-TRAF3IP2 fusion protein with TRAF6 would be preserved and enable TRAF6 K63-linked polyubiquitination independent of the CBM signalosome to activate NF-kB.

To test this hypothesis, we substituted the acidic amino acid residues in the N-terminal TRAF6 binding motif (PVEVDE) with Ala residues (PVAVAA). While wild-type TRAF3IP2 and FYN-TRAF3IP2 co-immunoprecipitated with TRAF6, mutation of the TRAF6 binding motif (FYN-TRAF3IP2$^{\Delta T6}$) abrogated the interaction with TRAF6 and led to a decrease in K63-linked polyubiquitination of TRAF6 (Fig. 4a). In the opposite direction, co-immunoprecipitation of TRAF6 – including polyubiquitinated TRAF6 – with FYN-TRAF3IP2$^{\Delta T6}$ was attenuated (Fig. 4b). Contrary to Ba/F3 cells with expression of *FYN-TRAF3IP*, Ba/F3 cells with ectopic expression of *FYN-TRAF3IP2*$^{\Delta T6}$ (**Supplementary Fig. 3c**) did not grow out after withdrawal of IL-3 (Fig. 4c). Expression of *FYN-TRAF3IP2*$^{\Delta T6}$ in Jurkat cells or primary CD4$^{+}$ T cells (**Supplementary Fig. 3c**) impaired activation of the canonical NF-kB pathway (Fig. 4d-e).

To investigate whether FYN-TRAF3IP2 could activate the NF-kB pathway independent of CARD11, we generated *CARD11* knock-out Jurkat cells with CRISPR/Cas9 genome editing (**Supplementary Fig. 3d-e**). Expression of *FYN-TRAF3IP2*, but not *TRAF3IP2* or *FYN-TRAF3IP2*$^{\Delta T6}$ augmented NF-kB transcriptional activity in resting conditions in both wild-type and *CARD11* knock-out Jurkat cells. Activation of PKCq with phorbol 12-myristate 13-acetate (PMA) and ionomycin increased NF-kB transcriptional activity in wild-type Jurkat cells, but significantly more in Jurkat cells with expression of *FYN-TRAF3IP2*. CARD11 deficiency impaired NF-kB activation in response to PMA and ionomycin, but *CARD11* knock-out Jurkat cells with *FYN-TRAF3IP2* expression remained significantly more responsive to PMA/ ionomycin stimulation than empty vector control or cells with expression of *TRAF3IP2* or *FYN-TRAF3IP2*$^{\Delta T6}$. This proves that FYN-TRAF3IP2 does not require the CBM signalosome, but suggests an interaction – direct or indirect – between FYN-TRAF3IP2 and PKCq.

Collectively, these results indicate that FYN-TRAF3IP2 directly interacts with TRAF6 and activates TRAF6 and the NF-kB pathway without intervention of the CBM signalosome.

## FYN-TRAF3IP2 expression causes PTCL-NOS-like disease in vivo

To test the oncogenic potential of the fusion protein *in vivo*, we transduced lineage negative hematopoietic stem and progenitor cells (HSPC) from wild-type mice with either the empty pMIG vector or the pMIG vector containing *FYN-TRAF3IP2* or *FYN*$^{G2A}$*-TRAF3IP2*. Subsequently, we injected the transduced cells (**Supplementary Fig. 4a**) intravenously in sublethally irradiated syngeneic recipient mice. Engraftment rates were comparable (**Supplementary Fig. 4b**). As early as 7 weeks after transplantation, GFP$^{+}$ cells in the peripheral blood of mice transplanted with HSPC expressing *FYN-TRAF3IP2* skewed towards CD4$^{+}$ cells (**Supplementary Fig. 4c**). Mice with expression of *FYN-TRAF3IP2* in hematopoietic cells, started losing weight 8 weeks after transplantation and succumbed within 16 weeks after transplantation (Fig. 5a). These mice had splenomegaly (Fig. 5b) and generalized lymphadenopathy. In

contrast, mice transplanted with cells expressing mutant *FYN$^{G2A}$-TRAF3IP2* did not develop disease (Fig. 5a,b). Lymph nodes from mice with *FYN-TRAF3IP2*-expressing cells displayed an effaced lymph node architecture with paracortical expansion and loss of germinal centers. The lymph nodes contained medium-sized and large cells with irregular, pleomorphic nuclei and multiple, prominent nucleoli. Malignant cells were surrounded by a polymorphic infiltrate with numerous eosinophils and histiocytes (Fig. 5c). *FYN-TRAF3IP2*-driven lymphomas were invariably CD4$^+$ (Fig. 5d). These cells were also found in the spleens (**Supplementary Fig. 4d**) and infiltrated the livers (Fig. 5e-f). *FYN-TRAF3IP2* and *FYN$^{G2A}$-TRAF3IP2* were expressed in lymph nodes (Fig. 5g) and *FYN-TRAF3IP2* expression was restricted to GFP$^+$ cells (**Supplementary Fig. 4e**). Analysis of *Tcrb* locus rearrangements with RT-PCR corroborated the clonal nature of the disease (Fig. 5h).

Because we identified *FYN-TRAF3IP2* gene fusions in both PTCL-NOS and PTCL-TFH, we determined the immunophenotype of murine *FYN-TRAF3IP2*-driven lymphomas. Malignant cells were positive for PD-1 and ICOS, but negative for the $T_{fh}$ marker CXCR5 (Fig. 6a). The BCL6 transcription factor orchestrates $T_{fh}$ identity, but was not expressed in *FYN-TRAF3IP2*-induced lymphomas (Fig. 6b). B cell proliferation with an expansion of germinal center (GC) B cells and plasma cells frequently accompanies $T_{fh}$-related neoplasms. In contrast, we observed a reduction in B cells in *FYN-TRAF3IP2*-associated lymphomas (Fig. 6c) without an increased proportion of GC B cells (Fig. 6d). The presence of plasma cells was more variable, but overall, not significantly altered (Fig. 6e). Consistent with the histologic finding of an increased number of histiocytes and eosinophils, the proportion of CD11b$^+$ myeloid cells was increased in *FYN-TRAF3IP2*-driven lymphomas (**Supplementary Fig. 4f**). The fraction of CD4$^+$ cells was increased in *FYN-TRAF3IP2* driven lymphomas and there were no changes in the number of CD8$^+$ cells (**Supplementary Fig. 4f**). Finally, there was no proliferation of high endothelial venules (Fig. 6f). These results are compatible with PTCL-NOS rather than PTCL-TFH.

Collectively, these *in vivo* data indicate that *FYN-TRAF3IP2* is a disease driver in PTCL-NOS and that the oncogenic potential of the FYN-TRAF3IP2 fusion protein is critically dependent on its anchored location to the plasma membrane because lymphomagenesis was abolished in *FYN$^{G2A}$-TRAF3IP2*-expressing cells.

**FYN-TRAF3IP2-driven lymphomas have active NF-kB signaling and are sensitive to inhibition of BCL-$X_L$**

We compared the gene expression profile of sorted CD4$^+$GFP$^+$ lymphoma cells with naive CD4$^+$ T cells, CD4$^+$GFP$^-$ non-malignant stromal T cells from the lymphoma and CD4$^+$GFP$^+$ *FYN$^{G2A}$-TRAF3IP2*-expressing T cells. Consistent with the neoplastic nature of the disease, numerous cell-cycle-associated genes were among the most significantly upregulated genes in *FYN-TRAF3IP2*-expressing lymphoma cells (**Supplementary Fig. 5a**). Overexpression of *Icos* and *Pdcd1* was congruent with the immunophenotype determined with flow cytometry. Additionally, lymphoma cells overexpressed *Runx2* and *Id2*. Both genes oppose the $T_{fh}$ phenotype and are repressed by *Bcl6*[23], in support of a non-$T_{fh}$ origin of the lymphomas (**Supplementary Fig. 5a**). We analyzed the cis-regulatory features associated with differentially expressed genes to identify the transcription factors driving these phenotypes with i-

cisTarget. This analysis consistently retrieved the NF-kB1 motif and the PU.1 motif as the most significantly enriched cis-regulatory features associated with overexpressed genes in *FYN-TRAF3IP2*-expressing lymphoma cells (Fig. 7a). Gene set enrichment analysis (GSEA) for different p65 (RelA) target gene gene sets reaffirmed increased expression of canonical NF-kB target genes in *FYN-TRAF3IP2*-expressing cells (Fig. 7b). As expected, malignant cells expressed *Relb* – a known direct transcriptional target of p50/p65[24] (**Supplementary Fig. 5b**). However, there was no enrichment of RelB target genes in malignant cells (**Supplementary Fig. 5c**) and RelB was sequestered in the cytosol of *FYN-TRAF3IP2*-expressing cells (**Supplementary Fig. 5b**). The transcription factor PU.1 (also known as SPI1) has been associated with the $T_h9$ phenotype. The cytokine profile of *FYN-TRAF3IP2*-expressing lymphoma cells was compatible with a $T_h9$ phenotype[25] (**Supplementary Fig. 5d**). Consistent with *in vitro* assays, there was no univocal activation of MAPK signaling in *FYN-TRAF3IP2*-expressing cells. The AP-1 motif was associated with cis-regulatory features of upregulated genes in lymphoma cells versus naive $CD4^+$ T cells and downregulated genes in lymphoma cells versus *FYN$^{G2A}$-TRAF3IP2*-expressing $CD4^+$ T cells (Fig. 7a). Likewise, GSEA for c-Jun target genes yielded inconsistent results (**Supplementary Fig. 5e**).

Targeting NF-kB directly for clinical purposes remains elusive because of on-target toxicities. This prompted us to examine vulnerabilities downstream of NF-kB. Promoting cell survival through induction of target genes, is one of the best documented functions of NF-kB[26]. Indeed, pro-survival and to a lesser extent pro-apoptotic factors were upregulated in *FYN-TRAF3IP2*-expressing cells (Fig. 8a). We reasoned that inhibition of pro-survival signals could tilt the balance towards apoptosis. BCL-$X_L$ (encoded by the *Bcl2l1*) gene was consistently overexpressed by lymphoma cells at both the RNA level and protein level in our mouse model (Fig. 8a-b). BCL-$X_L$ expression was also confirmed in case PTCL2 (Fig. 8c). Compared to naive $CD4^+$ T cells cultured under identical conditions, *FYN-TRAF3IP2*-expressing cells were > 30-fold more sensitive to inhibition of BCL-$X_L$, BCL-W and BCL2 with ABT-263 treatment (Fig. 8d).

These results demonstrate that *FYN-TRAF3IP2* activates NF-kB signaling *in vivo* and that this confers malignant cells with vulnerability to inhibition of BCL-$X_L$.

**KHDRBS1-LCK mediates chronic active TCR signaling**

We cloned the open reading frame of the *KHDRBS1-LCK* fusion transcript derived from patient cDNA in the pMIG vector to study the signaling properties of the KHDRBS1-LCK fusion protein. Here, the kinase domain of LCK was fused to the KHDRBS1 dimerization domain. It thus lacks the nuclear localization signal of KHDRBS1 and the membrane localization motif of LCK (Fig. 1c), suggesting that this protein functions in the cytosol. Indeed, in primary T cells with ectopic expression of *KHDRBS1-LCK*, the fusion protein accumulated in the cytosol when compared to T cells with ectopic expression of *LCK* (Fig. 9a). Retroviral transduction of IL-3 dependent Ba/F3 cells with *KHDRBS1-LCK* (**Supplementary Fig. 6a**) led to IL-3 independent growth *in vitro* and this was abolished by an inactivating LCK kinase domain mutation (*KHDRBS1-LCK$^{K273R}$*)[27] (Fig. 9b**)**. Likewise, inhibition of LCK kinase activity with dasatinib could efficiently block the proliferation of transformed Ba/F3 cells at low nanomolar concentrations (Fig. 9c). KHDRBS1-LCK but not KHDRBS1-LCK$^{K273R}$ was constitutively active (Tyr394 phosphorylation) in unstimulated

Jurkat cells (Fig. 9d). Likewise, proximal TCR signaling was significantly enhanced in primary T cells with expression of *KHDRSB1-LCK* in resting conditions and after TCR stimulation compared to primary T cells transduced with empty pMIG vector or *LCK* (Fig. 9e). Inhibition of LCK kinase activity with dasatinib reverted these differences (Fig. 9e). Further downstream of the TCR, KHDRBS1-LCK activated MAPK signaling and this was inhibited by dasatinib (Fig. 9f).

Collectively, these data show that KHDRBS1-LCK is a constitutively active tyrosine kinase which leads to chronic active TCR signaling.

### KHDRBS1-LCK instigates PTCL-NOS in vivo

To test the oncogenic potential of *KHDRBS1-LCK in vivo*, we transduced HSPC from wild-type mice with MSCV retrovirus with either an empty pMIG vector or a pMIG vector containing the *KHDRBS1-LCK* ORF. We observed incomplete disease penetrance (Fig. 10a). One mouse developed a lymphoproliferative disorder with generalized lymphadenopathy, moderate splenomegaly, pleural effusion and thymic enlargement, but no leukocytosis (**Supplementary Fig. 6b**). Normal tissue architecture was effaced. Residual follicles were pushed to the border of the lymph nodes. The expanded paracortex was dominated by a monotonous proliferation of medium-sized lymphocytes with irregular nuclei with 1 or 2 nucleoli and an increased number of blood vessels (Fig. 10b). Malignant cells were $CD4^{-}CD8^{+}$ and the majority expressed surface TCRb (Fig. 10c, **Supplementary Fig. 6c**). Bone marrow infiltration was limited. Negativity for TdT ruled out a lymphoblastic lymphoma/leukemia (Fig. 10d). Lymphomas expressed the KHDRBS1-LCK fusion protein, which was highly phosphorylated (Fig. 10e). Interestingly, also endogenous LCK was highly phosphorylated in lymphomatous spleens compared to spleens from empty pMIG vector mice despite comparable LCK protein levels, hinting at activation of endogenous LCK by KHDRBS1-LCK.

## Discussion

Recent advances on the genetics of PTCL-NOS have not led to tangible results for the development of novel therapeutic strategies. On the other hand, a handful of therapies (e.g. romidepsin[28]) is successful in a minority of patients with PTCL-NOS, but insight in their mechanism of activity is lacking. In this study, we have identified two novel gene fusions in PTCL-NOS that could function as novel targets for therapy. We have studied their activity in T cell models, both *in vitro* and *in vivo*, and we were able to show that both gene fusions confer therapeutic vulnerability to clinically available compounds.

We identify and characterize here a recurrent *FYN-TRAF3IP2* gene fusion in PTCL-NOS and PTCL-TFH. Despite the apparent heterogeneity of PTCL-NOS, the *FYN-TRAF3IP2* gene fusion ranks as one of the most recurrent events identified to date in this disease. To gain insight in the biology of malignant cells, efforts have been made to establish a cell of origin for different T cell lymphomas. PTCL-NOS has been divided in subgroups based on the expression of the $T_h2$-related transcription factor *GATA3* or the $T_h1$- and cytotoxic-T-cell-related transcription factors *TBX21* and *EOMES*[4]. In our mouse model there was

evidence for a $T_h9$-related signature in *FYN-TRAF3IP2*-driven lymphomas. Except for one $CD8^+$ and one CD4/CD8 double-negative PTCL-NOS, all human samples with a *FYN-TRAF3IP2* gene fusion were $CD4^+$.

FYN-TRAF3IP2 activates canonical NF-kB signaling to exert its oncogenic effects. Activation of NF-kB by both cell-intrinsic events and cell-extrinsic cues is well described for various B cell lymphomas and multiple myeloma[7]. On the contrary, the contribution of NF-kB signaling to T cell lymphomagenesis remains ill-defined. The relative contribution of canonical and non-canonical NF-kB signaling to PTCL-NOS biology remains largely unresolved and studies reached conflicting conclusions[29,30]. Mechanistic studies provided evidence for both pathways in molecularly defined subsets of PTCL. In ATLL, *PRKCB* mutations activate canonical NF-kB[31] and IRF4 and p65 jointly dictate super enhancer formation[32]. On the other hand, non-canonical NF-kB signaling is activated downstream of CD30 in $CD30^+$ PTCL[33]. In ALCL, RelB enhances transcriptional activation by *NFKB2-ROS1* gene fusions[12] and STAT3 drives the expression of *CD30* and *NFKB2*[34]. Overexpression of *GAPDH* in T cells, leads to a PTCL-TFH-like disease in mice which is largely driven by non-canonical NF-kB signaling[35]. We show that the oncogenic properties of FYN-TRAF3IP2 are primarily determined by its ability to activate canonical NF-kB without a significant contribution of non-canonical NF-kB.

In physiological circumstances, TRAF3IP2-dependent signaling is initiated after recruitment to the plasma membrane upon IL-17 receptor engagement[18]. We show that the FYN-TRAF3IP2 fusion protein undergoes acylation at the FYN-derived N-terminal SH4-domain. This post-translational modification anchors the protein to the plasma membrane and renders it constitutively active. We identify the canonical NF-kB pathway as the prime target of FYN-TRAF3IP2. Likewise, the pleckstrin homology domain of ITK directs the ITK-SYK fusion protein to the plasma membrane leading to constitutive SYK kinase activity and chronic active TCR signaling in PTCL-TFH[8]. Unlike ITK-SYK, FYN-TRAF3IP2 does not have kinase activity, but acts as a signaling adaptor and has E3 ubiquitin ligase activity[22]. Together with the Ubc13-Uev1A E2 complex, FYN-TRAF3IP2 will catalyze K63-linked polyubiquitination of TRAF6. K63-linked polyubiquitinated TRAF6 will activate the IKK and TAK1 kinase complexes. Phosphorylation by these complexes, will mark IkB for proteasomal degradation thereby releasing NF-kB transcription factors. These are now free to translocate to the nucleus and initiate transcription. Importantly, our data suggest that the direct interaction between FYN-TRAF3IP2 and TRAF6 will bypass most of the paradigmatic TCR cascade, including the CBM signalosome.

Several outstanding questions remain to be answered. First, the *FYN-TRAF3IP2* gene fusion appears specific for mature T cell neoplasms. It was not identified in recent large-scale studies of mature B cell neoplasms[36–38]. A concurrent report confirms that the *FYN-TRAF3IP2* gene fusion is a T-cell-lymphoma-exclusive event[39]. In our mouse model all mice invariably developed $CD4^+$ T cell lymphomas despite constitutive expression of the fusion protein in all hematopoietic lineages. T cell specificity could be related to interactions of the FYN-TRAF3IP2 protein with T cell specific partners. Indeed, the SH4 domain of FYN can interact directly with CD3z[40]. Therefore, it is plausible that the FYN-TRAF3IP2 fusion protein preferentially partitions to TCR cluster regions in the plasma membrane, facilitating the activation of

downstream pathways through vicinity. Our data suggest that FYN-TRAF3IP2-initiated signaling bypasses proximal TCR components such as ZAP70. Further downstream in the TCR cascade, *FYN-TRAF3IP2*-expressing cells display enhanced responsiveness to activation of PKCq by PMA/ionomycin, but do not require the CBM signalosome to activate TRAF6. Rather FYN-TRAF3IP2 interacts directly with TRAF6 to activate canonical NF-kB signaling. From these observations, it is reasonable to assume that FYN-TRAF3IP2 requires proximity to the TCR complex to activate NF-kB. FYN-TRAF3IP2-dependent signaling appears to bypass much of the TCR cascade, but our findings could point at a crosstalk between both pathways at the levels of the TCR complex and PKCq. Putative interactions of FYN-TRAF3IP2 with the TCR complex and PKCq warrant further exploration.

In all experiments, we observed comparably lower levels of the FYN-TRAF3IP2 fusion protein than mutant variants of the fusion protein. This could not be related to lower mRNA expression, because the fusion protein was expressed along with GFP from a bicistronic vector and we observed no decrease of the GFP protein (Fig. 5g). These observations suggest that levels of the FYN-TRAF3IP2 fusion protein are likely controlled by post-transcriptional regulation and/or post-translational regulation. Persistent activation of TRAF3IP2 by IL-17 desensitizes cells through degradation of TRAF3IP2 orchestrated by Skp1-cullin-1-F-box-type (SCF) E3 ubiquitin ligase complexes[41]. It is unknown whether levels of active FYN-TRAF3IP2 protein are regulated similarly by SCF-type E3 ubiquitin ligase complexes. Secondary lesions which impact FYN-TRAF3IP2 protein turnover, could enhance lymphomagenesis. The number of sequenced samples in this study did not allow statistical inference to identify events that co-occur with a *FYN-TRAF3IP2* gene fusion, but this will be of interest for future research.

Direct targeting of NF-kB signaling with IKK inhibitors has shown promise in preclinical models, but to date no IKK inhibitors are in clinical use. On one hand, they exhibit limited efficacy. On the other hand, they provoke prohibitive on-target toxicities related, but not limited, to the ubiquitous activity of the NF-kB pathway in both the innate and adaptive immune system[42]. Therefore, we shifted our focus to downstream effectors of the NF-kB pathway. The ability of NF-kB to promote cell survival through induction of target genes is well-described[26]. With the notable exception of *Mcl1*, we observed a global upregulation of pro-survival factors in murine lymphomas induced by *FYN-TRAF3IP2*. The expression of pro-apoptotic factors *Bax*, *Bak1*, BH3-only activators and BH3-only sensitizers was elevated to a lesser extent (Fig. 8a). *Bcl2l1* was one of the most significantly upregulated pro-survival genes. Expression of its gene product BCL-$X_L$ was confirmed in malignant cells in murine lymphomas and in a clinical specimen with a *FYN-TRAF3IP2* gene fusion. Given the increased expression of pro-apoptotic factors in *FYN-TRAF3IP2*-driven murine lymphomas, we reasoned that these cells are primed for apoptosis[43]. Indeed, *FYN-TRAF3IP2*-dependent lymphoma cells display exquisite sensitivity to the BCL-$X_L$, BCL2 and BCL-W (encoded by *Bcl2l2*) inhibitor ABT-263. ABT-263 is in clinical development for the treatment of myelofibrosis. Thrombocytopenia is the most important side effect of BCL-$X_L$, but is manageable with appropriate dosing. Moreover, a BCL-$X_L$ proteolysis targeting chimera is in development. This compound is more potent than ABT-263 at inhibiting BCL-$X_L$ while at the same time it minimizes toxicity to

thrombocytes[44]. Considering the importance of NF-kB in the regulation of cell survival, these results provide a strong rationale to target BCL-$X_L$ in *FYN-TRAF3IP2*-driven lymphomas.

In addition to the recurrent *FYN-TRAF3IP2* fusion, we identified a *KHDRBS1-LCK* fusion, which represents a prototypic fusion kinase. In resting T cells, a significant fraction of LCK is catalytically active[45] through autophosphorylation of tyrosine 394 in the LCK activation loop[46]. The KHDRBS1-LCK fusion protein bears the KHDRBS1 dimerization domains[17], which could enhance LCK transphosphorylation and activation. Indeed, constitutive dimerization of a tyrosine kinase domain by fusion with a self-associating partner protein is a recurrent mechanism in oncogenic fusion proteins and was able to activate LCK in an insertion mutagenesis screen[47]. We show that KHDRBS1-LCK kinase activates different branches of the TCR signaling cascade. We provide evidence that targeting LCK kinase activity with dasatinib has potent inhibitory effects on KHDRBS1-LCK-driven signaling, paving the way for therapeutic intervention in a clinical setting. Early-stage clinical trials suggest activity of dasatinib in PTCL-NOS[48] and TFH-related PTCL[49]. With the identification of the *KHDRBS1-LCK* gene fusion, we provide an additional biological basis to repurpose dasatinib for the treatment of PTCL-NOS.

Together, our data provide novel genetic and biologic insight in PTCL-NOS and PTCL-TFH as well as a rationale for the design of novel treatment regimens for PTCL cases with these fusion genes. Overall, these data warrant further study of abnormal TCR signaling in PTCL.

# Declarations


## ACKNOWLEDGEMENTS

This work was supported by Fonds Tom Debackere voor Lymfoomonderzoek and Stichting Tegen Kanker (2018/1272). The Leica SP8x confocal microscope was provided by InfraMouse (KU Leuven-VIB) through a Hercules type 3 project (ZW09-03). K.D. holds a PhD fellowship aspirant of Fonds Wetenschappelijk Onderzoek Vlaanderen (FWO, 1147319N) and an Emmanuel van der Schueren fellowship from Kom Op Tegen Kanker. S.D. holds a post-doctoral fellowship from Stichting Tegen Kanker.


## AUTHOR CONTRIBUTIONS

K.D. conceived the project, collected clinical samples, performed bioinformatic analysis, planned and performed experiments, interpreted data and wrote the manuscript; L.M., M.v.B., N.M., O.G., K.J. and M.B. performed experiments; S.D. performed bioinformatic analysis; G.G., L.M., C.G. and I.W. provided clinical samples; P.G., L.d.L. and T.T. provided clinical samples and reviewed histopathology; J.C. and D.D. supervised the project, planned experiments, interpreted data and wrote the manuscript.

## COMPETING INTERESTS

D.D. holds a chair funded by Roche.

# References


1. Parrilla Castellar, E.R. *et al.* ALK-negative anaplastic large cell lymphoma is a genetically heterogeneous disease with widely disparate clinical outcomes. *Blood* **124**, 1473-80 (2014).
2. Vose, J., Armitage, J., Weisenburger, D. & International, T.C.L.P. International peripheral T-cell and natural killer/T-cell lymphoma study: pathology findings and clinical outcomes. *J Clin Oncol* **26**, 4124-30 (2008).
3. d'Amore, F. *et al.* Peripheral T-cell lymphomas: ESMO Clinical Practice Guidelines for diagnosis, treatment and follow-up. *Ann Oncol* **26 Suppl 5**, v108-15 (2015).
4. Heavican, T.B. *et al.* Genetic drivers of oncogenic pathways in molecular subgroups of peripheral T-cell lymphoma. *Blood* **133**, 1664-1676 (2019).
5. Laginestra, M.A. *et al.* Whole exome sequencing reveals mutations in FAT1 tumor suppressor gene clinically impacting on peripheral T-cell lymphoma not otherwise specified. *Mod Pathol* **33**, 179-187 (2020).
6. Watatani, Y. *et al.* Molecular heterogeneity in peripheral T-cell lymphoma, not otherwise specified revealed by comprehensive genetic profiling. *Leukemia* **33**, 2867-2883 (2019).
7. Nagel, D., Vincendeau, M., Eitelhuber, A.C. & Krappmann, D. Mechanisms and consequences of constitutive NF-kappaB activation in B-cell lymphoid malignancies. *Oncogene* **33**, 5655-65 (2014).
8. Pechloff, K. *et al.* The fusion kinase ITK-SYK mimics a T cell receptor signal and drives oncogenesis in conditional mouse models of peripheral T cell lymphoma. *J Exp Med* **207**, 1031-44 (2010).
9. An, J. *et al.* Truncated ERG Oncoproteins from TMPRSS2-ERG Fusions Are Resistant to SPOP-Mediated Proteasome Degradation. *Mol Cell* **59**, 904-16 (2015).
10. Mertens, F., Johansson, B., Fioretos, T. & Mitelman, F. The emerging complexity of gene fusions in cancer. *Nat Rev Cancer* **15**, 371-81 (2015).
11. Abate, F. *et al.* Activating mutations and translocations in the guanine exchange factor VAV1 in peripheral T-cell lymphomas. *Proc Natl Acad Sci U S A* **114**, 764-769 (2017).
12. Crescenzo, R. *et al.* Convergent mutations and kinase fusions lead to oncogenic STAT3 activation in anaplastic large cell lymphoma. *Cancer Cell* **27**, 516-32 (2015).
13. Debackere, K. *et al.* FER and FES tyrosine kinase fusions in follicular T-cell lymphoma. *Blood* **135**, 584-588 (2020).
14. Kuefer, M.U. *et al.* Retrovirus-mediated gene transfer of NPM-ALK causes lymphoid malignancy in mice. *Blood* **90**, 2901-10 (1997).
15. Agnelli, L. *et al.* Identification of a 3-gene model as a powerful diagnostic tool for the recognition of ALK-negative anaplastic large-cell lymphoma. *Blood* **120**, 1274-81 (2012).
16. Vasmatzis, G. *et al.* Genome-wide analysis reveals recurrent structural abnormalities of TP63 and other p53-related genes in peripheral T-cell lymphomas. *Blood* **120**, 2280-9 (2012).

17. Feracci, M. *et al.* Structural basis of RNA recognition and dimerization by the STAR proteins T-STAR and Sam68. *Nat Commun* **7**, 10355 (2016).
18. Li, X., Bechara, R., Zhao, J., McGeachy, M.J. & Gaffen, S.L. IL-17 receptor-based signaling and implications for disease. *Nat Immunol* **20**, 1594-1602 (2019).
19. Alland, L., Peseckis, S.M., Atherton, R.E., Berthiaume, L. & Resh, M.D. Dual myristylation and palmitylation of Src family member p59fyn affects subcellular localization. *J Biol Chem* **269**, 16701-5 (1994).
20. Rawlings, D.J., Sommer, K. & Moreno-Garcia, M.E. The CARMA1 signalosome links the signalling machinery of adaptive and innate immunity in lymphocytes. *Nat Rev Immunol* **6**, 799-812 (2006).
21. Ryzhakov, G., Blazek, K. & Udalova, I.A. Evolution of vertebrate immunity: sequence and functional analysis of the SEFIR domain family member Act1. *J Mol Evol* **72**, 521-30 (2011).
22. Liu, C. *et al.* Act1, a U-box E3 ubiquitin ligase for IL-17 signaling. *Sci Signal* **2**, ra63 (2009).
23. Choi, J. *et al.* Bcl-6 is the nexus transcription factor of T follicular helper cells via repressor-of-repressor circuits. *Nat Immunol* **21**, 777-789 (2020).
24. Bren, G.D. *et al.* Transcription of the RelB gene is regulated by NF-kappaB. *Oncogene* **20**, 7722-33 (2001).
25. Chang, H.C. *et al.* The transcription factor PU.1 is required for the development of IL-9-producing T cells and allergic inflammation. *Nat Immunol* **11**, 527-34 (2010).
26. Baud, V. & Karin, M. Is NF-kappaB a good target for cancer therapy? Hopes and pitfalls. *Nat Rev Drug Discov* **8**, 33-40 (2009).
27. Levin, S.D., Anderson, S.J., Forbush, K.A. & Perlmutter, R.M. A dominant-negative transgene defines a role for p56lck in thymopoiesis. *EMBO J* **12**, 1671-80 (1993).
28. Piekarz, R.L. *et al.* Phase 2 trial of romidepsin in patients with peripheral T-cell lymphoma. *Blood* **117**, 5827-34 (2011).
29. Martinez-Delgado, B. *et al.* Differential expression of NF-kappaB pathway genes among peripheral T-cell lymphomas. *Leukemia* **19**, 2254-63 (2005).
30. Odqvist, L. *et al.* NIK controls classical and alternative NF-kappaB activation and is necessary for the survival of human T-cell lymphoma cells. *Clin Cancer Res* **19**, 2319-30 (2013).
31. Kataoka, K. *et al.* Integrated molecular analysis of adult T cell leukemia/lymphoma. *Nat Genet* **47**, 1304-15 (2015).
32. Wong, R.W.J. *et al.* Feed-forward regulatory loop driven by IRF4 and NF-kappaB in adult T-cell leukemia/lymphoma. *Blood* **135**, 934-947 (2020).
33. Boddicker, R.L. *et al.* The oncogenic transcription factor IRF4 is regulated by a novel CD30/NF-kappaB positive feedback loop in peripheral T-cell lymphoma. *Blood* **125**, 3118-27 (2015).
34. Wang, H. *et al.* A novel model of alternative NF-kappaB pathway activation in anaplastic large cell lymphoma. *Leukemia* (2020).

35. Mondragon, L. *et al.* GAPDH Overexpression in the T Cell Lineage Promotes Angioimmunoblastic T Cell Lymphoma through an NF-kappaB-Dependent Mechanism. *Cancer Cell* **36**, 268-287 e10 (2019).
36. Arthur, S.E. *et al.* Genome-wide discovery of somatic regulatory variants in diffuse large B-cell lymphoma. *Nat Commun* **9**, 4001 (2018).
37. Bea, S. *et al.* Uniparental disomies, homozygous deletions, amplifications, and target genes in mantle cell lymphoma revealed by integrative high-resolution whole-genome profiling. *Blood* **113**, 3059-69 (2009).
38. Panea, R.I. *et al.* The whole-genome landscape of Burkitt lymphoma subtypes. *Blood* **134**, 1598-1607 (2019).
39. Moon, C.S. *et al.* FYN–TRAF3IP2 induces NF-κB signaling-driven peripheral T-cell lymphoma. *Nature Cancer* **2**, 98-113 (2021).
40. Timson Gauen, L.K., Kong, A.N., Samelson, L.E. & Shaw, A.S. p59fyn tyrosine kinase associates with multiple T-cell receptor subunits through its unique amino-terminal domain. *Mol Cell Biol* **12**, 5438-46 (1992).
41. Shi, P. *et al.* Persistent stimulation with interleukin-17 desensitizes cells through SCFbeta-TrCP-mediated degradation of Act1. *Sci Signal* **4**, ra73 (2011).
42. Prescott, J.A. & Cook, S.J. Targeting IKKbeta in Cancer: Challenges and Opportunities for the Therapeutic Utilisation of IKKbeta Inhibitors. *Cells* **7**(2018).
43. Singh, R., Letai, A. & Sarosiek, K. Regulation of apoptosis in health and disease: the balancing act of BCL-2 family proteins. *Nat Rev Mol Cell Biol* **20**, 175-193 (2019).
44. Khan, S. *et al.* A selective BCL-XL PROTAC degrader achieves safe and potent antitumor activity. *Nat Med* **25**, 1938-1947 (2019).
45. Gaud, G., Lesourne, R. & Love, P.E. Regulatory mechanisms in T cell receptor signalling. *Nat Rev Immunol* **18**, 485-497 (2018).
46. Veillette, A. & Fournel, M. The CD4 associated tyrosine protein kinase p56lck is positively regulated through its site of autophosphorylation. *Oncogene* **5**, 1455-62 (1990).
47. Lierman, E., Van Miegroet, H., Beullens, E. & Cools, J. Identification of protein tyrosine kinases with oncogenic potential using a retroviral insertion mutagenesis screen. *Haematologica* **94**, 1440-4 (2009).
48. Umakanthan, J.M. *et al.* Phase I/II study of dasatinib and exploratory genomic analysis in relapsed or refractory non-Hodgkin lymphoma. *Br J Haematol* **184**, 744-752 (2019).
49. Nguyen, T.B. *et al.* Dasatinib Is an Effective Treatment for Angioimmunoblastic T-cell Lymphoma. *Cancer Res* **80**, 1875-1884 (2020).

# Figures


## Figure 1

FYN-TRAF3IP2 and KHDRBS1-LCK gene fusions in PTCL-NOS. a Schematic depiction of the protein structure and Sanger sequencing of the RT-PCR amplicon for the FYN-TRAF3IP2 fusion in the PTCL-NOS case (PTCL2, left) and the PTCL-TFH case (FTCL4, right). b Sanger sequencing of the genomic DNA amplicon for the PTCL-NOS case (PTCL2). c Schematic depiction of the protein structure and Sanger sequencing of the RT-PCR amplicon for the KHDRBS1-LCK fusion.

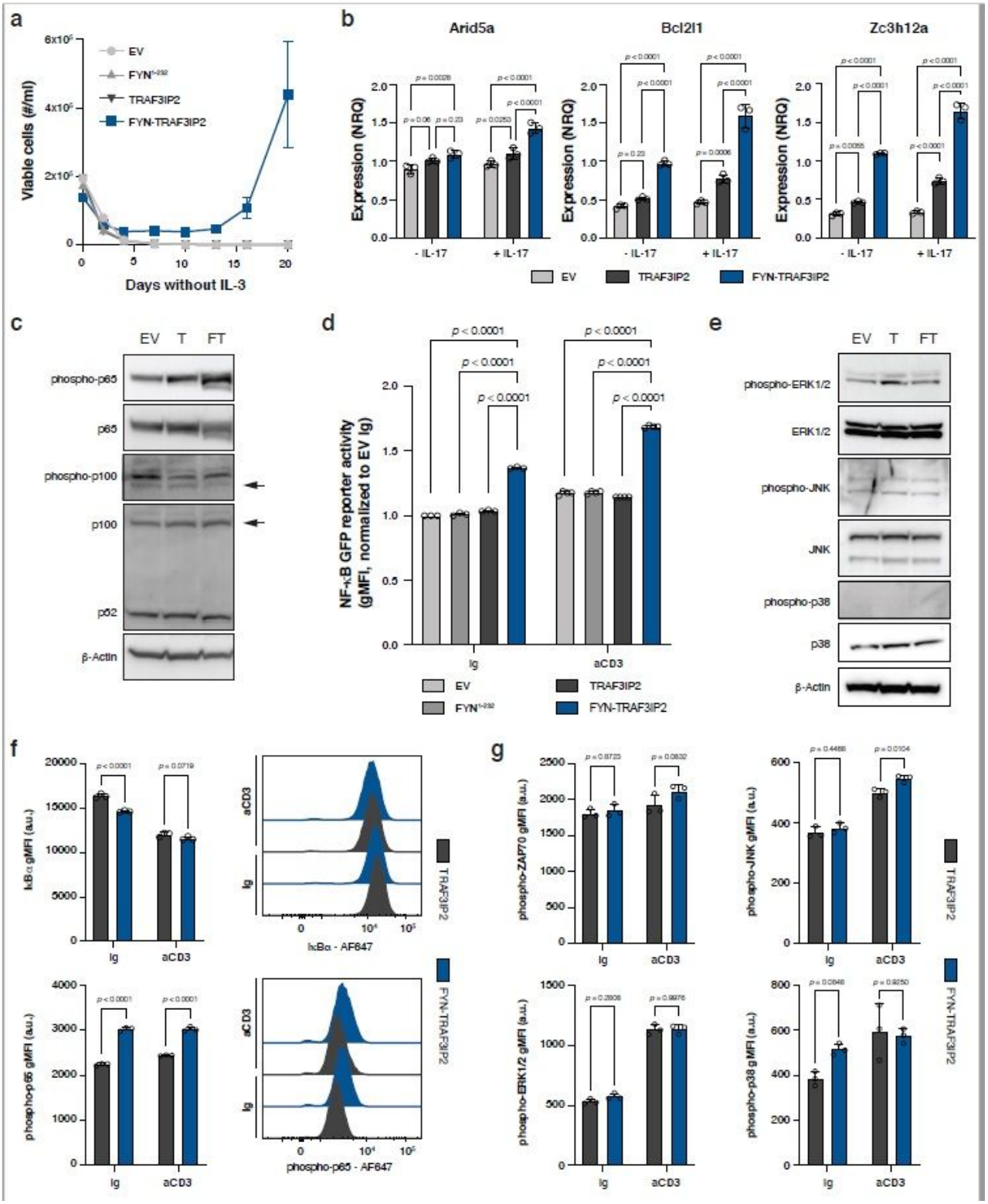


## Figure 2

FYN-TRAF3IP2-dependent signaling intersects with TCR signaling. a Outgrowth of Ba/F3 cells transduced with empty pMIG vector, pMIG-FYN1-232, pMIG-TRAF3IP2 or pMIG-FYN-TRAF3IP2 after withdrawal of IL-3. n = 3 biological replicates per condition. b qRT-PCR for IL-17-regulated transcripts in naive CD4+ T cells transduced with empty pMIG vector, pMIG-TRAF3IP2 or pMIG-FYN-TRAF3IP2. n = 3 biological replicates per condition. p-values were calculated with Tukey's post-hoc multiple comparisons test. c Western blot

analysis for canonical and non-canonical NF-kB activation in Jurkat cells transduced with empty pMIG vector, pMIG-TRAF3IP2 or pMIG-FYN-TRAF3IP2. d NF-kB GFP reporter signal intensity in Jurkat cells with empty control vector or expression of FYN1-232, TRAF3IP2 or FYN-TRAF3IP2 after stimulation with an agonistic anti-CD3e antibody or exposure to control immunoglobulin (Ig). n = 3 biological replicates per condition for Ig control, n = 4 for anti-CD3e. p-values were calculated with Tukey's post-hoc multiple comparisons test. e Western blot analysis for activation of MAPK pathways in Jurkat cells transduced with empty pMIG vector, pMIG-TRAF3IP2 or pMIG-FYN-TRAF3IP2. f Intracellular flow cytometry for IkBa (top row) or phospho-p65 (bottom row) in CD4+ T cells treated with control immunoglobulin (Ig) or agonistic anti-CD3e antibody. n = 3 biological replicates per condition. p-values were calculated with Tukey's post-hoc multiple comparisons test. g Intracellular flow cytometry proximal TCR signaling and MAPK pathway activation in CD4+ T cells treated with control immunoglobulin (Ig) or agonistic anti-CD3e antibody. n = 3 biological replicates per condition. p-values were calculated with Tukey's post-hoc multiple comparisons test. All data are represented as mean ± standard deviation (SD).

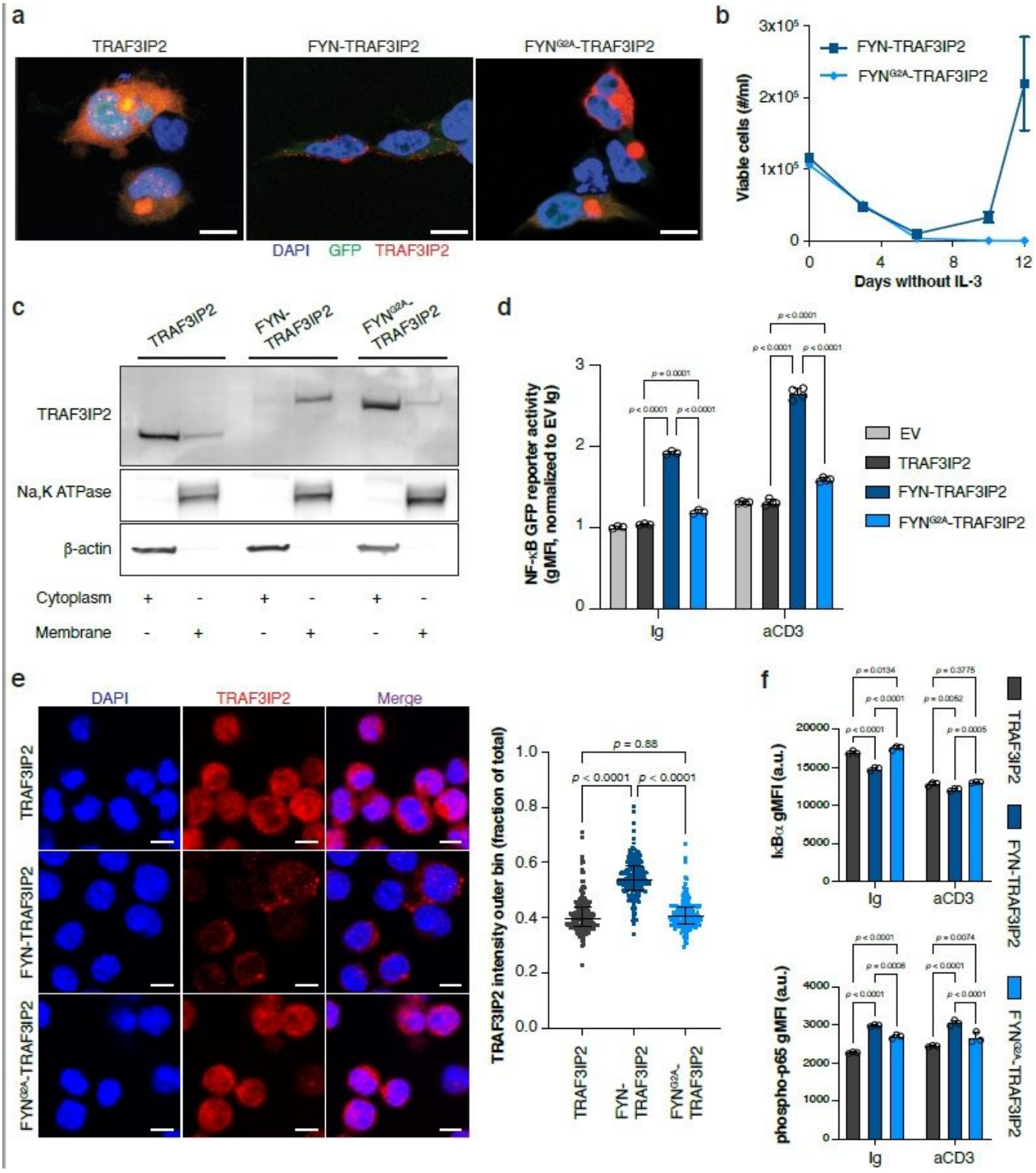


## Figure 3

Membrane anchoring of FYN-TRAF3IP2 is required to activate NF-kB signaling. a Immunofluorescence images of 293T cells transfected with TRAF3IP2, FYN-TRAF3IP2 and FYNG2A-TRAF3IP2 stained for TRAF3IP2. Scalebars represent 10 µm. b Outgrowth of Ba/F3 cells transduced with pMIG-FYN-TRAF3IP2 or pMIG-FYNG2A-TRAF3IP2 after withdrawal of IL-3. n = 3 biological replicates per condition. c Western blot analysis for TRAF3IP2 on cytoplasmic and membrane fractions of Jurkat cells transduced with

pMIG-TRAF3IP2, pMIG-FYN-TRAF3IP2 and pMIG-FYNG2A-TRAF3IP2. d NF-kB GFP reporter signal intensity in Jurkat cells with empty control vector or expression of TRAF3IP2, FYN-TRAF3IP2 or FYNG2A-TRAF3IP2 after stimulation with an agonistic anti-CD3e antibody or exposure to control immunoglobulin (Ig). n = 3 biological replicates per condition for Ig control, n = 4 for anti-CD3e. p-values were calculated with Tukey's post-hoc multiple comparisons test. e Immunofluorescence images (left) of TRAF3IP2 staining on CD4+ T cells transduced to express TRAF3IP2, FYN-TRAF3IP2 or FYNG2A-TRAF3IP2. Scalebars represent 5 μm. Quantification (right) of TRAF3IP2 signal intensity in the outer cell bin, expressed as fraction of signal intensity over the entire cell. Each dot represents a cell. Horizontal line and whiskers represent median and interquartile range respectively. p-values were calculated with Games-Howell's multiple comparisons test. f Intracellular flow cytometry for IkBa (top row) or phospho-p65 (bottom row) in CD4+ T cells treated with control immunoglobulin (Ig) or agonistic anti-CD3e antibody. n = 3 biological replicates per condition. p-values were calculated with Tukey's post-hoc multiple comparisons test.All data are represented as mean ± SD unless stated otherwise.

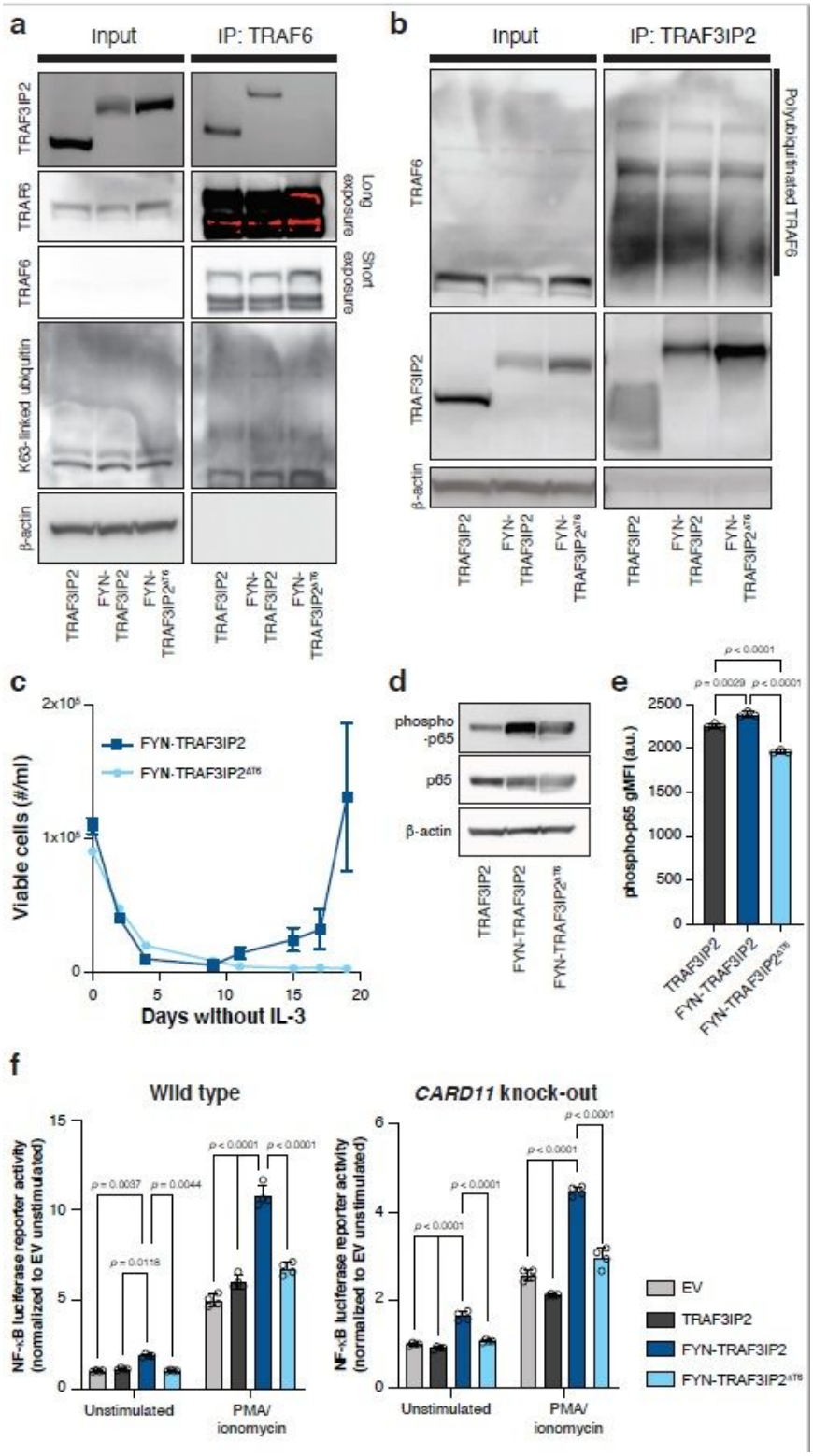


## Figure 4

FYN-TRAF3IP2 activates TRAF6 and canonical NF-kB signaling independent of the CBM signalosome. a Western blot analysis of whole-cell lysate and anti-TRAF6 immunoprecipitate in TRAF3IP2-, FYN-TRAF3IP2- and FYN-TRAF3IP2ΔT6-expressing Jurkat cells. b Western blot analysis of whole-cell lysate and anti-TRAF3IP2 immunoprecipitate in TRAF3IP2-, FYN-TRAF3IP2- and FYN-TRAF3IP2ΔT6-expressing Jurkat cells. c Outgrowth of Ba/F3 cells transduced with pMIG-FYN-TRAF3IP2 or pMIG-FYN-

TRAF3IP2ΔT6 after withdrawal of IL-3. n = 3 biological replicates per condition. d Western blot analysis for canonical NF-kB activation in Jurkat cells transduced with pMIG-TRAF3IP2, pMIG-FYN-TRAF3IP2 or pMIG-FYN-TRAF3IP2ΔT6. e Intracellular flow cytometry for phospho-p65 in resting CD4+ T cells with expression of TRAF3IP2, FYN-TRAF3IP2 or FYN-TRAF3IP2ΔT6. n = 3 biological replicates per condition. p-values were calculated with Tukey's post-hoc multiple comparisons test. f NF-kB luciferase reporter signal intensity in wild-type Jurkat cells (left) or CARD11 knock-out Jurkat cells (right) with empty control vector or expression of TRAF3IP2, FYN-TRAF3IP2 or FYN-TRAF3IP2ΔT6 in resting conditions or after stimulation with PMA. n = 4 biological replicates per condition. p-values were calculated with Tukey's post-hoc multiple comparisons test. All data are represented as mean ± SD.

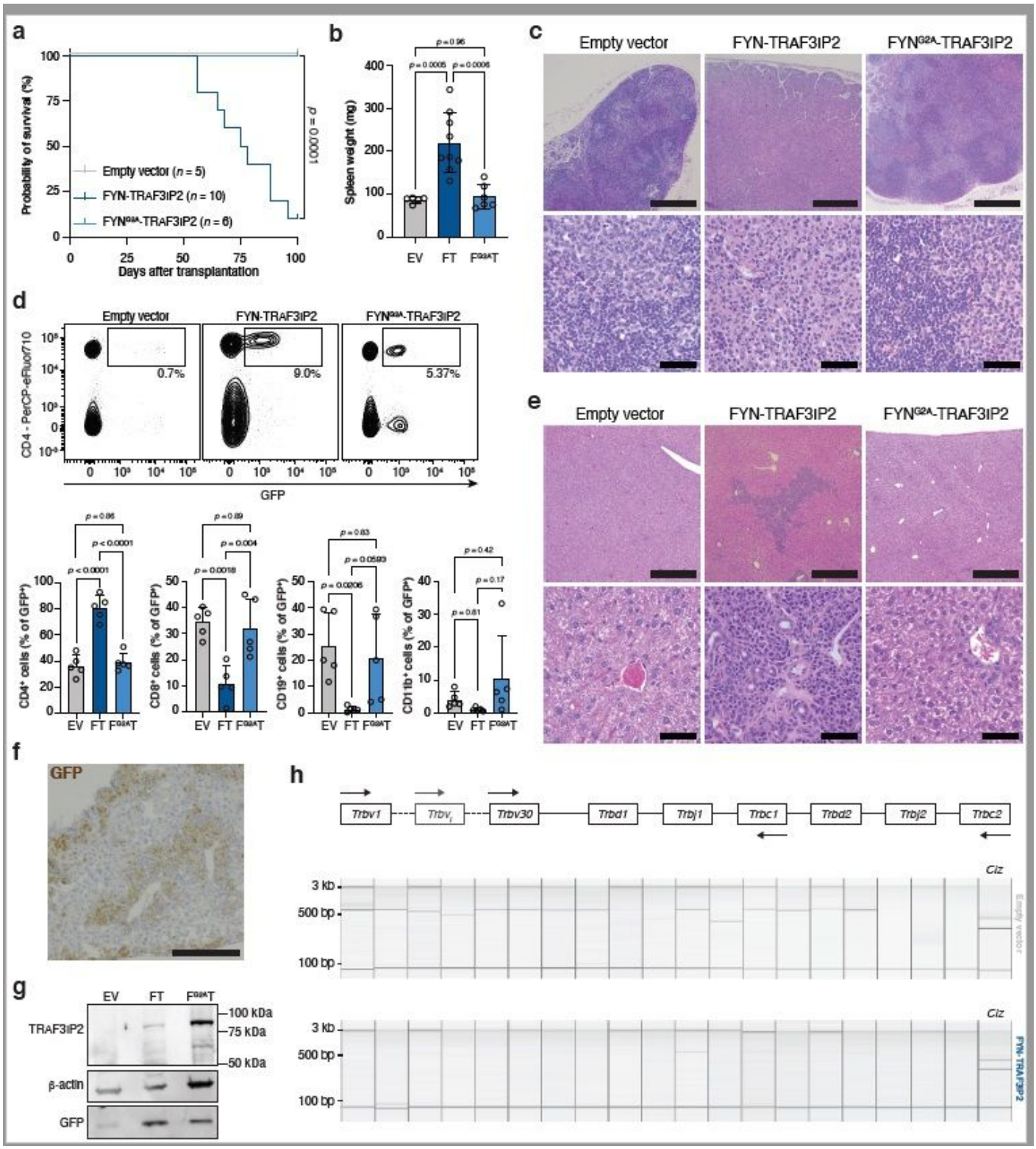


## Figure 5

Expression of FYN-TRAF3IP2 in hematopoietic cells fosters the development of PTCL-NOS. a Kaplan-Meier survival curve after transplantation with HSPC transduced with empty pMIG vector (n = 5), pMIG-FYN-TRAF3IP2 (n = 10) or pMIG-FYNG2A-TRAF3IP2-GFP (n = 6). p-value was calculated with Mantel-Cox test. b Spleen weights at sacrifice of mice transplanted with HSPC transduced with empty pMIG vector (EV, n = 5), pMIG-FYN-TRAF3IP2 (FT, n = 9) or pMIG-FYNG2A-TRAF3IP2 (FG2AT, n = 6). p-values were

calculated with Tukey's post-hoc multiple comparisons test. c Representative H&E stains of lymph nodes from mice transplanted with HSPC transduced with empty vector (n = 5), FYN-TRAF3IP2 (n = 5) or FYNG2A-TRAF3IP2 (n = 5). Low magnification images are in the top row, scalebars represent 500 μm. High magnification images are in the bottom row, scalebars represent 50 μm. d Representative flow cytometry plots for cell suspensions from the lymph nodes of EV mice, FT mice and FG2AT mice (top). Quantification of the lineage of GFP+ cells in lymph node cell suspensions (bottom). n = 5 mice per group. p-values were calculated with Tukey's post-hoc multiple comparisons test. e Representative H&E stains of livers from mice transplanted with HSPC transduced with empty vector (n = 5), FYN-TRAF3IP2 (n = 5) or FYNG2A-TRAF3IP2 (n = 5). Low magnification images are in the top row, scalebars represent 500 μm. High magnification images are in the bottom row, scalebars represent 50 μm. f Representative picture of GFP immunohistochemistry on liver sections of mice with FYN-TRAF3IP2-expressing cells (n = 5). Scalebar represents 200 μm. g Western blot analysis for TRAF3IP2 and GFP on lymph node lysates after transplantation with HSPC transduced with empty vector, pMIG-FYN-TRAF3IP2 or pMIG-FYNG2A-TRAF3IP2. h Representative gel analysis pictures for RT-PCR analysis of Tcrb rearrangements (left to right: Trbv6, Trbv1, Trbv26, Trbv2, Trbv12-1/12-2/12-3, Trbv19, Trbv29, Trbv13-1/13-2/13-3, Trbv17, Trbv4, Trbv16, Trbv15, Trbv14, Trbv31, Trbv20, Trbv3, Trbv18, Trbv30 and Trbv21) and Ciz control reaction (far right lane) on lymph nodes from an empty vector control mouse (top, n = 2) and a FYN-TRAF3IP2-induced lymphoma (bottom, n = 5). All data are represented as mean ± SD.

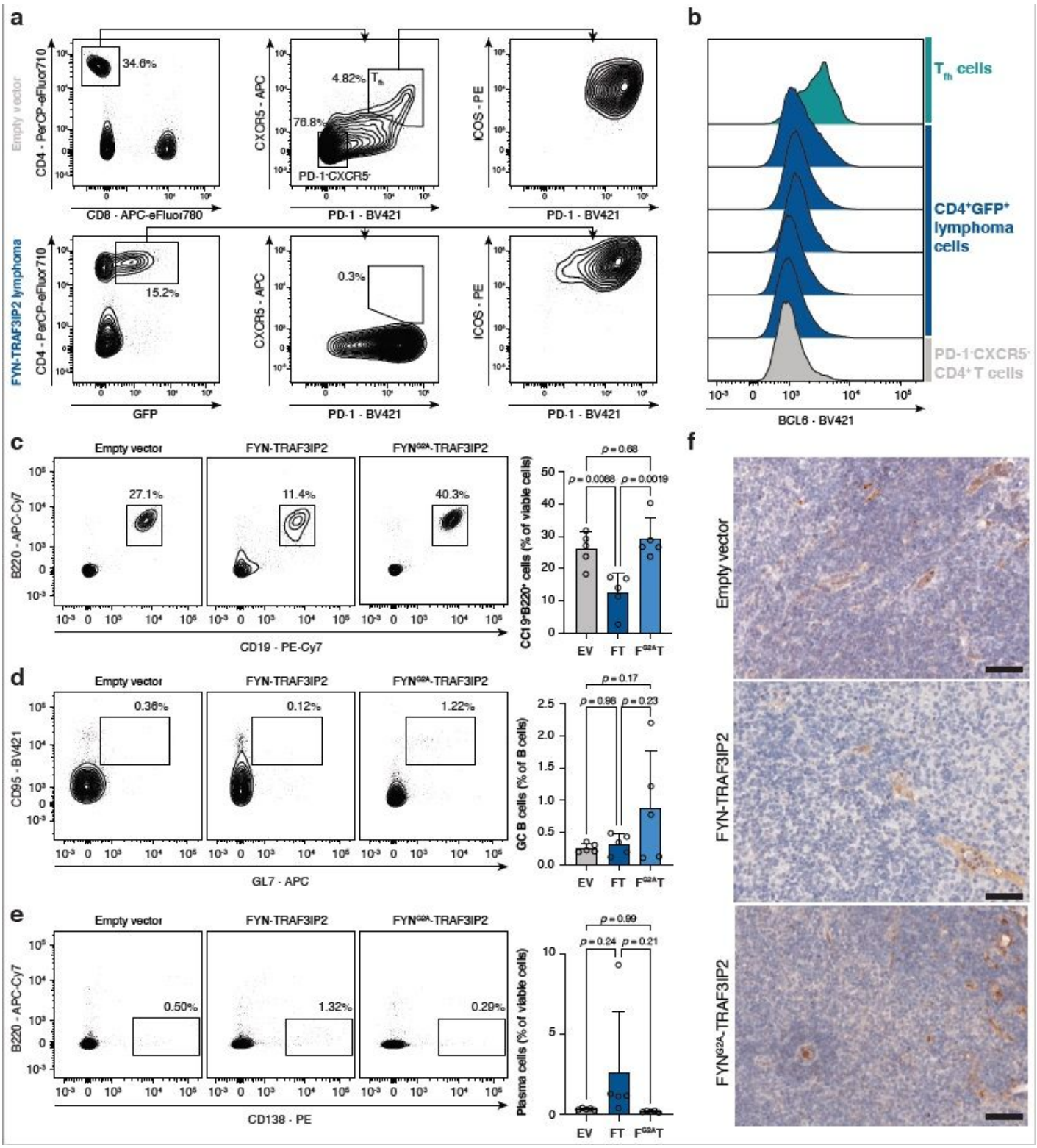


## Figure 6

Characterization of FYN-TRAF3IP2-driven lymphomas in mice. a Gating strategy for Tfh cells on lymph node cell suspensions from mice with empty-vector-transduced cells (top). Representative flow cytometry plot for the immunophenotype of FYN-TRAF3IP2-driven lymphomas (bottom, n = 9). b Histograms for BCL6 protein in Tfh cells (representative for n = 2), sorted viable CD4+GFP+ splenocytes from FYN-TRAF3IP2-driven lymphomas (n = 5) and PD-1-CXCR5- CD4+ T cells (representative for n = 2). c, d, e

Representative flow cytometry plots (left) and quantification (right) of CD19+B220+ B cells (c), CD95+GL7+ germinal center (GC) B cells (gated on CD19+B220+ B cells) (d) and CD19lo-intB220lo-intCD138+ plasma cells (e) in lymph node suspensions from mice transplanted with empty-vector-transduced (EV) cells, FYN-TRAF3IP2-transduced (FT) cells or FYNG2A-TRAF3IP2-transduced cells (FG2AT). n = 5 mice per group. p-values were calculated with Tukey's post-hoc multiple comparisons test. f Representative pictures of CD31 immunohistochemistry on lymph node sections of mice transplanted with HSPC transduced with empty pMIG vector, pMIG-FYN-TRAF3IP2 or pMIG-FYNG2A-TRAF3IP2. n = 5 mice per group. Scalebars represent 50 µm. Data are represented as mean ± SD.

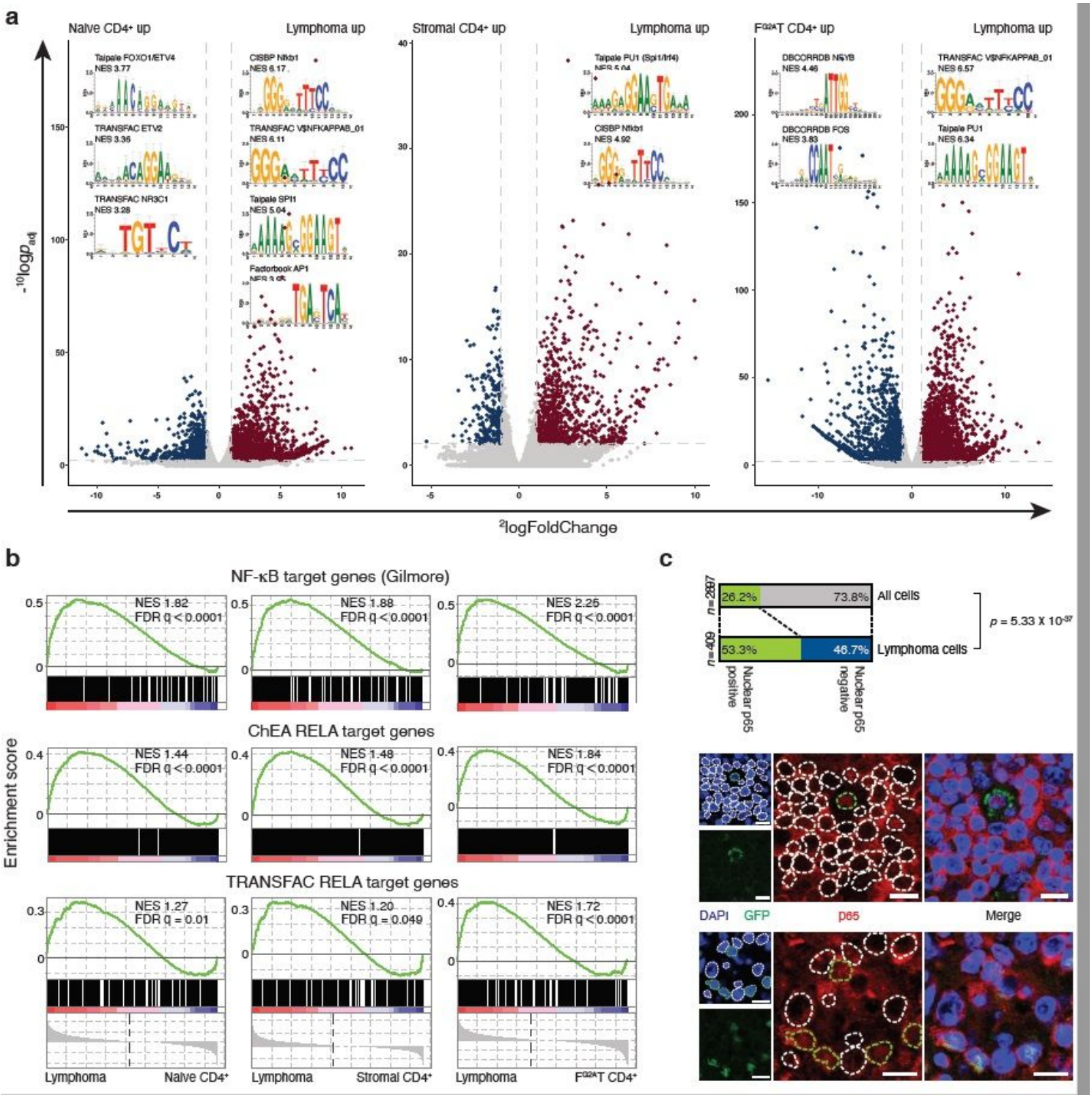

## Figure 7

FYN-TRAF3IP2 activates canonical NF-kB signaling in vivo. a Volcano plots of differentially expressed genes in CD4+GFP+ lymphoma cells versus naive CD4+ T cells (left), CD4+GFP- stromal T cells (middle) and CD4+GFP+ FYNG2A-TRAF3IP2-expressing T cells (right). Genes significantly upregulated (2logFoldChange > 1 and -10logpadj > 2) in lymphoma cells are maroon-colored, genes significantly downregulated (2logFoldChange < -1 and -10logpadj > 2) in lymphoma cells are depicted in blue. Motifs from cis-regulatory features associated with differentially expressed genes are depicted. b Enrichment plots for a list of manually curated NF-kB target genes (top row), p65 target genes identified by ChIP-seq (middle row) and computationally predicted p65 target genes (bottom row) in lymphoma cells compared with naive CD4+ T cells (left column), CD4+GFP- stromal T cells (middle column) and CD4+GFP+ FYNG2A-TRAF3IP2-expressing T cells (right column). c Quantification of cells with nuclear p65 positivity as a fraction of all cells in the lymphoma or as a fraction of GFP+ lymphoma cells in FYN-TRAF3IP2-induced lymphomas (top) and representative images (bottom). n = 5 mice. p-value is derived from the cumulative distribution function of a hypergeometric distribution. Scalebars represent 10 μm.

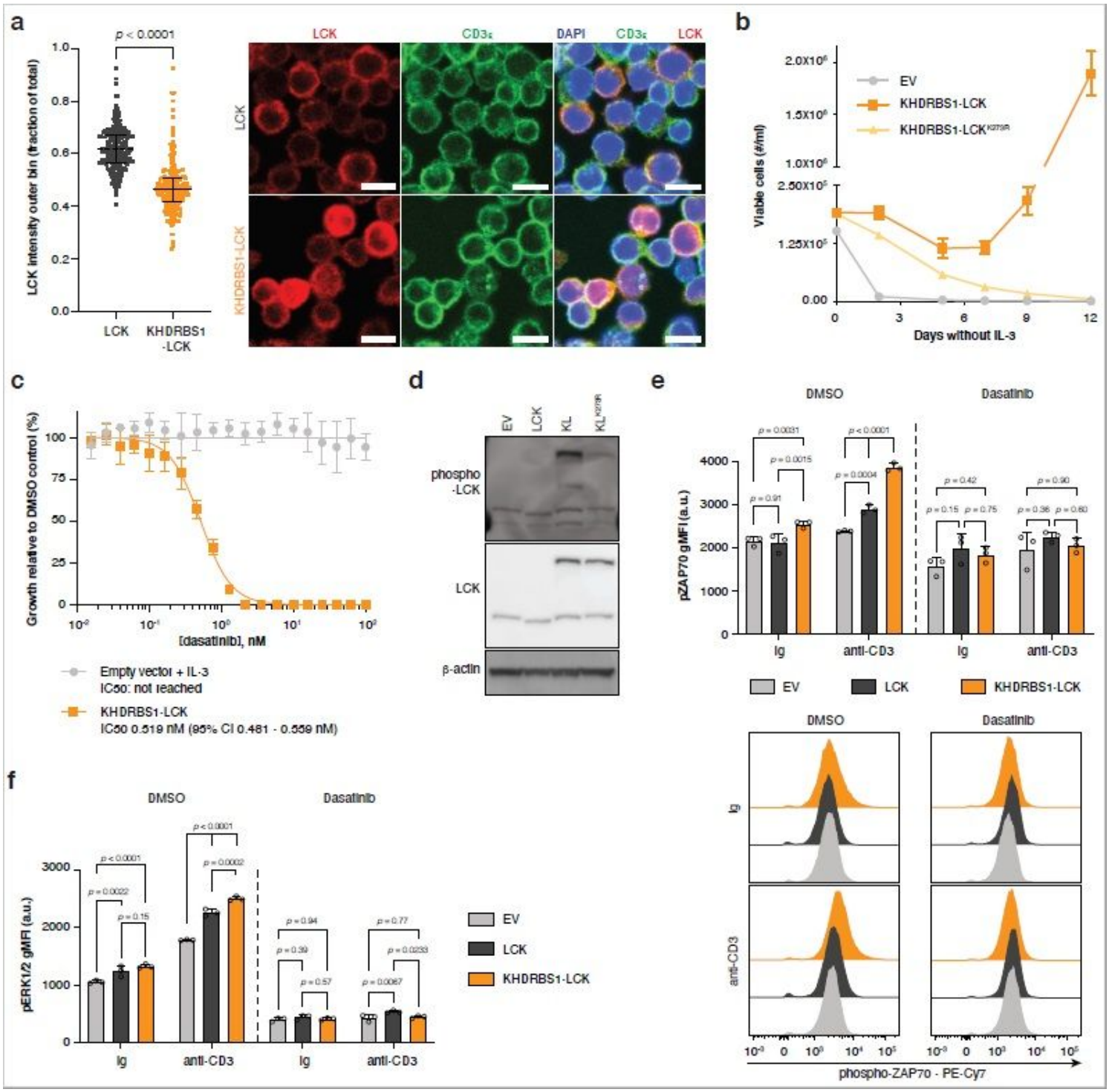


## Figure 9

KHDRBS1-LCK drives chronic active TCR signaling. a Quantification (left) and representative immunofluorescence images (right) of LCK and CD3e staining on primary T cells with ectopic expression of LCK or KHDRBS1-LCK. Each dot represents a cell. Horizontal line and whiskers represent median and interquartile range respectively. p-values were calculated with Mann-Whitney test. Scalebars represent 10 µm. b Outgrowth of Ba/F3 cells transduced with empty pMIG vector, pMIG-KHDRBS1-LCK or pMIG-KHDRBS1-LCKK273R after withdrawal of IL-3. n = 3 biological replicates per condition. c Growth inhibition of Ba/F3 cells transformed by KHDRBS1-LCK or Ba/F3 cells transduced with empty pMIG

vector after a 24-hour treatment with dasatinib. n = 3 replicates per condition. d Western blot for total LCK and phospho-LCK (Tyr394) in Jurkat cells transduced with empty pMIG vector, pMIG-LCK, pMIG-KHDRBS1-LCK or pMIG-KHDRBS1-LCKK273R. e Quantification (top) and representative flow cytometry histograms (bottom) for phospho-ZAP70 in primary T cells treated with control immunoglobulin (Ig) or agonistic anti-CD3e antibody in the absence or presence of dasatinib. n = 3 biological replicates per condition. p-values were calculated with Tukey's post-hoc multiple comparisons test. f Intracellular flow cytometry quantification of phospho-ERK1/2 levels in primary T cells treated with control immunoglobulin (Ig) or agonistic anti-CD3e antibody in the absence or presence of dasatinib. n = 3 biological replicates per condition. p-values were calculated with Tukey's post-hoc multiple comparisons test. All data are represented as mean ± SD unless stated otherwise.

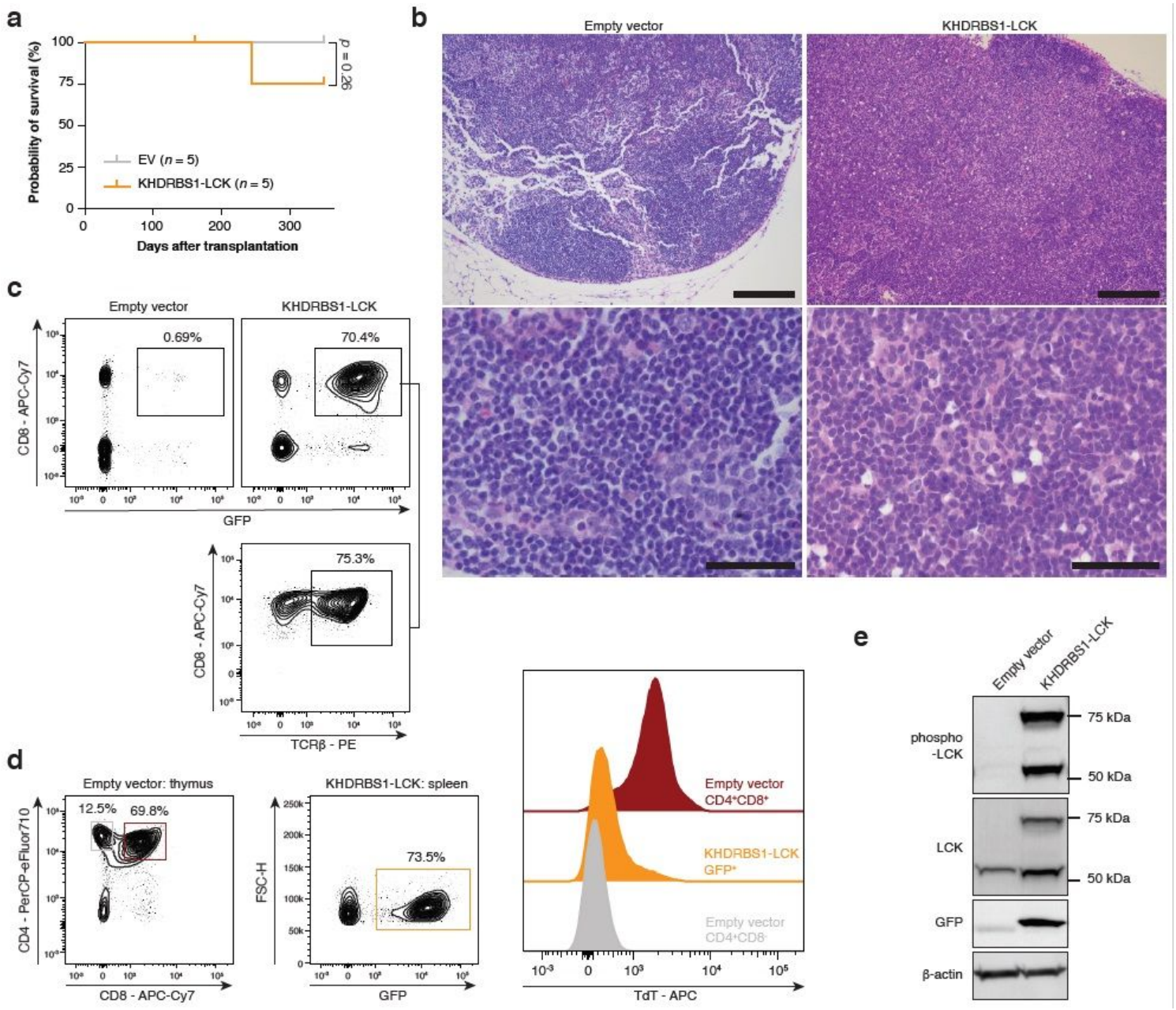


Figure 10

Characterization of KHDRBS1-LCK-driven PTCL in mice. a Kaplan-Meier survival curve after transplantation with HSPC transduced with empty pMIG vector (n = 5) or pMIG-KHDRBS1-LCK (n = 5). p-value was calculated with Mantel-Cox test. b Representative H&E stains of lymph nodes from mice who were transplanted with HSPC transduced with empty vector (n = 5) or KHDRBS1-LCK (n = 1). Low magnification images are in the top row, scalebars represent 200 μm. High magnification images are in the bottom row, scalebars represent 50 μm. c Representative flow cytometry plots for cell suspensions from the lymph nodes of empty vector mice (representative for n = 5) and the KHDRBS1-LCK mouse (n = 1). d Gating strategy for CD4+CD8+ double positive cells and CD4+CD8- single positive cells on thymic cell suspensions from mice with empty-vector-transduced cells and GFP+ cells in KHDRBS1-LCK induced PTCL (left). Quantification of intracellular TdT with intracellular flow cytometry. e Western blot for phospho-LCK (Tyr394) and total LCK in spleen lysates from mice transduced with HSPC transduced with empty vector or KHDRBS1-LCK-induced PTCL.

## Supplementary Files

This is a list of supplementary files associated with this preprint. Click to download.

- FigureS1.pdf
- FigureS2.pdf
- FigureS3.pdf
- FigureS4small.pdf
- FigureS5small.pdf
- FigureS6.pdf
- FigureS7.pdf
- SupplementaryTable1.xlsx
- SupplementaryTable2.xlsx
- KDBfusionsPTCLsupplementalrevisedfinal.docx